Long-Term Vibration Monitoring Onboard Mars Express Mission

Bortolino Saggin,* Diego Scaccabarozzi,† and Lorenzo Comolli‡
Politecnico di Milano, 23900 Lecco, Italy

This work describes mechanical vibration monitoring onboard the ESA Mars Express orbiter, in a period of eight years since the spacecraft commissioning. The vibrations are measured using the planetary Fourier spectrometer, an infrared spectrometer based on a modified Michelson interferometer, which is part of the mission payload. The instrument is very sensitive to thermomechanical inputs, and the mechanical vibrations are a source of disturbance for its scientific measurements. However, the instrument sensitivity to mechanical disturbances and the exploitation of a diagnostic mode provide a chance to monitor the vibration environment onboard the spacecraft. It has been assessed that the main vibration contributions derive from the reaction wheels and the laser ring gyroscopes that implement harmonic dithering. Spacecraft acceleration levels at the instrument mounting interface are provided with the aim of defining reference figures for engineers and scientists who have to cope with a usually unknown in-orbit vibration environment. Moreover, the vibration levels evolution along the mission lifetime is analyzed to highlight the effect of the spacecraft aging in that respect.

Nomenclature

a_i	=	acceleration amplitude along the direction i, m/s^2
f_k	=	fundamental frequency of reaction wheel k, Hz
f_j	=	excitation frequency for dwell sine excitation along direction j, Hz
I_{RW}	=	second-order momentum of the reaction wheel, kg m^2
M_{ang}	=	angular momentum of the reaction wheel, kg m^2 s^{-1}
$S_{i,j}$	=	vibration sensitivity for autotest mode along direction i at frequency j
$S_{\max}$	=	maximum vibration sensitivity for autotest mode
$S_{\min}$	=	minimum vibration sensitivity for autotest mode
$v_{i,j}$	=	speed derived from autotest measurement along direction i at frequency j, m/s

I. Introduction

INTEREST about characterization of the vibration environment onboard Earth observation satellites has grown since the early 1990s. In [1], the authors describe the result of in-orbit vibration assessment on the Olympus telecommunication satellite by means of an ultrasensitive triaxial accelerometer installed for the purpose of characterizing the satellite vibration environment, identifying the main sources of disturbance, and providing design data for sensitive optical payloads. The Micromedy experiment [2] launched in March 1998 was bound to defining the vibration environment and the spacecraft frequency response functions (FRFs) onboard the SPOT4 (Satellite Pour l'Observation de la Terre 4) satellite. The study reported slight changes of the spacecraft modes before and after launch and vibration levels within the 0.02 to 0.08 m/s^2 range,with relevant frequency components around 100 Hz. The Optical Inter-Orbits Communications Engineering Test Satellite (OICETS), launched in August 2005, included the microvibration equipment with a triaxial accelerometer for vibration monitoring at the mounting interface of the communication equipment LUCE during the whole in-orbit activity [3]. The authors evidenced a worsening of the vibration environment, with respect to the characterization performed on ground, with an rms acceleration level increase of about 0.1 m/s^2 on each measurement axis. Moreover, full compatibility between the FRFs measured on ground and in orbit was verified.

Despite the aforementioned cases, the opportunity to exploit accelerometers in order to monitor the in-orbit vibration environment on spacecraft and satellites is very rare, since priority is granted to the scientific experiments in the mass, power, and data rate budgets; this aspect is even more critical for missions operating far from the Earth where these resources are more scarce. In these cases, "devices" or instruments inadvertently sensitive to the mechanical disturbances are the only chance of achieving indirect information about the vibrations generated by the spacecraft. For instance, the authors in [4] showed how the microvibration environment onboard the Solar and Heliospheric Observatory (SOHO) spacecraft, launched in December 1995, can be retrieved by means of the image stabilization system (ISS) of the Michelson Doppler image instrument. The ISS is based on a gimballed mirror tilted by a rotational actuator for which the motion compensates the jitter generated by the spacecraft reaction wheels (RWs). Once the actuator current is converted into an angle, the vibration amplitude can be assessed.

The Mars Express (MEX) mission was the first planetary exploration mission of the ESA. MEX was successfully launched in June 2003 by a Soyuz–Fregat rocket and the orbit insertion at Mars was performed in December of the same year. During checkout, performed immediately after the launch when the satellite was still close to earth, the planetary fourier spectrometer (PFS) team [5,6] found that its measurements contained some unwanted features known as "ghosts" [7]; after some investigation, the effect was ascribed to the mechanical vibration present on the spacecraft [8].

Fourier interferometers are very sensitive to mechanical vibrations, and the PFS is not an exception [9] since any unwanted displacement of its optical components leaves a trace in measured spectra. The PFS sensitivity to mechanical vibrations was known before launch, but the assessment of the vibration levels at the mounting interface was, unfortunately, not performed because of the tight mission schedule. Moreover, the spacecraft was found to be noisier than expected and the mechanical disturbances were eventually a limitation for the PFS measurements.

Despite each satellite vibration environment being related to its peculiar characteristics (e.g., mechanical structure, instruments, mounting, and type of vibration sources), the acceleration levels obtained from the PFS measurements could be a starting point for engineers and scientists who have to design sensitive payloads but lack information about the expected vibration environment in the operative phase. Moreover, thanks to the large amount of data

*Professor, Mechanical Department, Lecco Campus, Polo Territoriale di Lecco; bortolino.saggin@polimi.it.

†Fellow Researcher, Mechanical Department, Lecco Campus, Polo Territoriale di Lecco; diego.scaccabarozzi@polimi.it.

‡Fellow Researcher, Mechanical Department, Lecco Campus, Polo Territoriale di Lecco; lorenzo.comolli@polimi.it.

retrieved by the PFS during these eight years, the tracking of the time evolution of the mechanical disturbances can be performed.

The paper is organized as follows: Section II describes the PFS sensitivity to mechanical disturbances and how these can be retrieved from its "autotest mode," whereas Sec. III provides the results of ground testing. Section IV shows the measured vibration environment in flight and its long-term evolution. In Sec. V, results are discussed, whereas Sec. VI finally concludes the paper.

II. PFS Mechanical Disturbances

A. Mechanical Vibration Sources

In [10], a review of possible (micro)vibration sources onboard satellites is carried out and many causes are investigated in depth. Moving parts of mechanisms, thermal effects [11], electromagnetic forces, thermal insulators buckling, and liquid or gaseous flows induce vibrations and shocks that are transmitted through the spacecraft structures. Besides the internal sources, many other external causes can be present, e.g., due to the release of thermally induced stresses or microshocks generated by impacts with space debris [12].

On MEX, the main source of mechanical vibrations was found to come from the gyroscopes in inertial measurement units (IMUs); their measurements being essential for the spacecraft attitude and orbit control system (AOCS), they must be continuously active. Six mechanically dithered ring laser gyroscopes (RLGs) [13,14], two for each axis for redundancy, are installed on the Mars Express orbiter and packed in two independent triaxial systems named IMU1 and IMU2. The dithering imposes harmonic oscillations of the RLG to avoid the drifts arousing when measuring angular speeds close to zero. MEX RLG dithering frequencies are in the range between 510 and 630 Hz.

Additional disturbances of lower amplitude come from the RWs (four on MEX orbiter) for which the features have been analyzed in various literature studies [15–21]. RWs generate vibrations in many different ways: flywheel static and dynamic imbalances produce vibrations at a base frequency corresponding to the nominal rotational speed and some other multiples [19]. Moreover, the fundamental frequency is generally time-varying as a consequence of the attitude control; and when it matches the resonances of the spacecraft structures, the disturbance is amplified and large vibration levels can be locally observed. The MEX RWs rotational speed is in the range of 0 to 200π rad/s; therefore, the fundamental frequency is expected to span from 0 to 100 Hz.

Ball-bearing disturbances are usually negligible if high-quality bearings are used; bearing excitation is typically a broadband white–noise-like disturbance if there is no localized defect on the rolling elements or on the races; nevertheless, they may cause narrowband vibrations because of the resonances of structural components.

B. PFS Sensitivity to Vibrations

The PFS is sensitive to mechanical vibrations that produce different effects on the measured spectra; a detailed description can be found in [22]. Here, a summary is proposed for convenience of the reader. The simplest effect is due to the piezoelectric sensitivity of most infrared detectors and, in particular, of the pyroelectric one. This effect is present on both PFS channels, i.e., long wavelength (LW) and short wavelength (SW), but it is quite useless if one wants to study mechanical vibrations. In the LW channel, the effect is superimposed on the large signal from Mars and, in most cases, is acquired in aliasing after the attenuation from the lowpass antialias filtering. In the SW channel, the PbSe detector piezoelectric sensitivity is very low below about 400 Hz and close to zero above.

Thus, the most effective way to evaluate vibrations is exploiting the interferogram modulation. Any optical signal detected by the interferometer is modulated with the moving mirror vibrations, incompletely compensated by the sampling strategy because of a time delay between the reference signal and the main interferogram. The reference laser-scattered light generates in the SW channel a strong spectral line positioned at the Nyquist wave number (i.e., 8400 cm^{-1}) and two ghost lines for each monoharmonic vibration, positioned symmetrically with respect to the reference laser wave number. The distance from the laser is proportional to the disturbance frequency, whereas the ghost amplitude is proportional to the vibration amplitude. In PFS, these lines are present in a spectral region (high wave numbers) where they are easily recognizable because the observed infrared light from Mars is smaller in comparison. Thanks to the analysis of the infrared spectrum, the mechanical disturbances can be monitored during the whole measurement session, lasting typically 1 or 2 h, allowing attention to be focused on the time-varying disturbances, like those coming from the RWs.

To avoid the "pollution" of the Martian spectra by the reference laser ghosts, the PFS team decided to switch off the SW laser since orbit 662 and, exploiting the redundancy provided by the reference laser of the LW channel, they used the latter also for the SW channel sampling. For that reason, the vibration monitoring based on the infrared spectrum analysis is limited only to the initial orbits.

C. PFS Autotest Mode

Autotest is a diagnostic mode designed to verify the correct interferometer mirror movement. In Fig. 1, a scheme of the procedure applied to derive the disturbance spectra is shown. The time intervals Δ_t between the zero crossings of a reference laser interferogram are recorded. The reference laser interferogram is modulated by the mirror's speed variations; therefore, any mechanical vibration changing the optical path difference (OPD) can be detected by analyzing the time difference between the recorded zero crossings. The scanning mirror speed is computed considering that each sampling point corresponds to a distance equal to half the reference laser wavelength λ_l. The computed speed, evenly sampled in OPD domain at constant steps, has to be resampled in the time domain. Finally, the speed frequency spectrum is obtained by applying the frequency Fourier transform (FFT) to the resampled speed. Figure 2a shows a zoom of the laser interferogram, whereas Fig. 2b shows the disturbance spectrum retrieved from the zero-crossings timings. Given the time length of the acquisition frame and the average sampling frequency, the spectrum extends up to 2500 Hz with a spectral resolution of about 0.6 Hz. For each measurement session, two autotests are typically taken, one at the beginning and one at the end of the operating phase. Thus, disturbances can be retrieved only at these occasions, typically a 1 or 2 h distant.

The spectrum of Fig. 2b is relative to the vibrations of the interferometer arms, but in order to compute the spacecraft transmitted spectrum, the instrument sensitivity has to be known.

III. PFS Vibration Sensitivity

A. Instrument Sensitivity

The PFS sensitivity to vibrations was experimentally determined, placing a special focus on the expected gyroscope and filter wheel disturbances. The test setup was based on a Bruel & Kjaer electrodynamic shaker, producing the desired excitation along three main mounting axes, as shown in Fig. 3a.

Acceleration and autotest data were recorded by a dedicated acquisition system. The tests were performed using dwell sine excitations with a frequency varying in the range of 60 to 1100 Hz and with an average base acceleration amplitude of 0.05 m/s^2. Three tests were run at each frequency in order to assess measurement repeatability, and the sensitivity along each direction was computed as

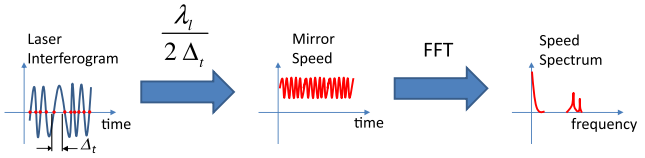

Fig. 1 Schematic of the procedure to derive speed disturbance spectrum.

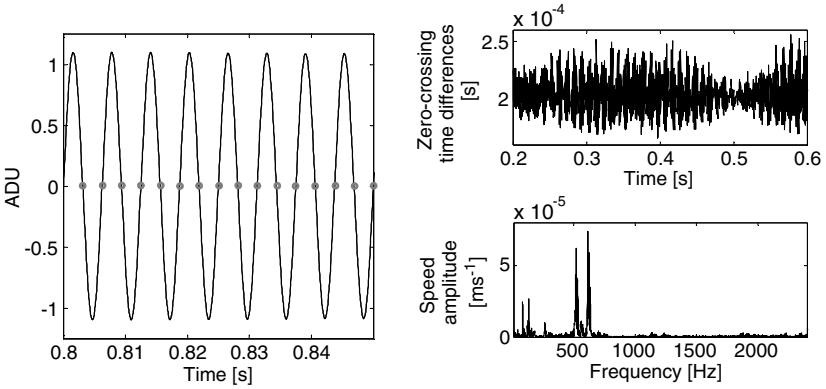

a) Reference laser interferogram versus time; zero crossings are evidenced as gray dots

b) Time differences between zero crossings (top) and speed spectrum (bottom)

Fig. 2 Interferogram sampling technique and vibration velocity spectrum.

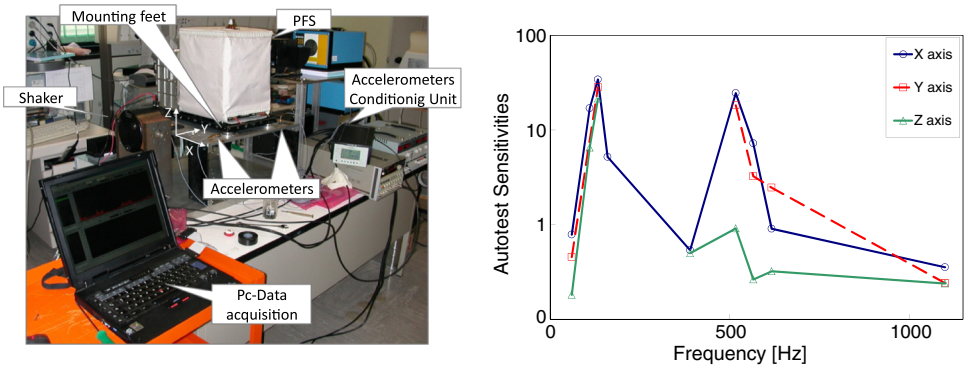

a) PFS qualification model and vibration measurement setup

b) PFS autotest sensitivities

Fig. 3 Experimental characterization of PFS mechanical vibration sensitivity. Sensitivities are in dimensionless units.

$$S_{i,j} = \frac{2\pi f_j v_{i,j}}{a_i} \tag{1}$$

The measured sensitivities along the reference system axes are shown in Fig. 3b. Repeatability was found to vary from 3 to 20% within the investigated frequency range.

Amplification was detected at 133 Hz. This derives from a resonance of the PFS scanning pendulum and, in particular, the mode shape is a bending of the pendulum arms. A second resonance was found at about 500 Hz. This amplification is present mainly along X and Y directions, whereas it is reduced by more than a factor of 10 along the Z axis. The resonance depends on the PFS mounting feet: these elements were designed to cut off high-acceleration levels above 100 Hz during the launch phase, but they are ineffective for the low vibration levels. In fact, they exploit dry friction to damp the vibration, and therefore their performances depend on the excitation level of the input. In the case of low-level vibrations, the static friction limit is not exceeded and the dampers behave like rigid bodies. This explains why the resonance at 133 Hz was excited in these tests, whereas during launch it had no effect.

The PFS autotest mode provides an indirect measurement of the disturbance, but it cannot determine the actual excitation direction. The difference between measured sensitivities for the Z axis (normal to the mounting plane) and the other axes is larger in the 500 Hz spectral region where the disturbances from gyroscopes are located. Thus, two sensitivities, named $S_{\max}$ and $S_{\min}$, were defined in order to estimate the minimum and maximum acceleration inputs from the spacecraft. For all the frequencies in which no information is available, a linear interpolation was applied. This procedure does not claim to be accurate, but it seems the only reasonable way to provide continuous information over the investigated spectral region.

B. PFS–Venus Express Ground Characterization

Microvibration assessment was, unfortunately, not performed on the PFS-MEX orbiter on ground because of the lack of time: matching the tight schedule was the priority, and mechanical disturbances were considered a minor issue.

Having the vibration issue raised on Mars Express, a microvibration test was performed on the Venus Express (VEX) spacecraft in Toulouse on November 2004, by Astrium. Venus Express was the first ESA mission to Venus [23], to investigate the planet's atmosphere and plasma environment. The VEX payload includes an infrared spectrometer nearly identical to PFS-MEX, both for mechanical structure and size. Moreover, the VEX orbiter is nearly identical to the MEX one; in particular, similar gyroscopes and reaction wheels were used.

The results of the microvibration assessment performed on the PFS-VEX payload therefore can be "reasonably" applied to the PFS-MEX case in order to compare the orbiter behavior before and after the launch.

The measurements were performed by means of two triaxial accelerometers fixed at the mounting interface between the spacecraft and the PFS-VEX, i.e., two dampers along one diagonal of the mounting interface. The accelerometers allowed measuring the acceleration levels along each mounting direction, i.e., the Z axis normal to the mounting interface, and the X and Y that lie on the mounting plane. The tests were performed by switching on all the gyroscopes. The sampling rate was set to 1600 Hz in each test. Table 2 provides the measured acceleration levels for each case.

Unfortunately, time series were not available, and therefore the disturbance spectra could not be computed, but the acceleration levels of Table 2 allow at least a comparison between on-ground and in-flight rms values.

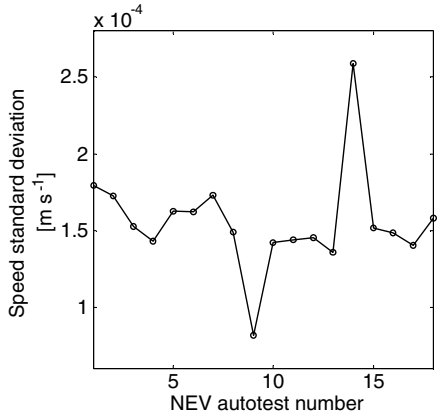

Fig. 4 Tracking of the standard deviation of the scanning speed during NEV phase.

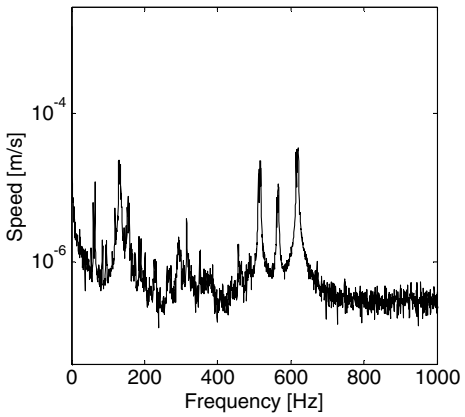

Fig. 5 Speed average spectrum of NEV autotests up to 1000 Hz frequency.

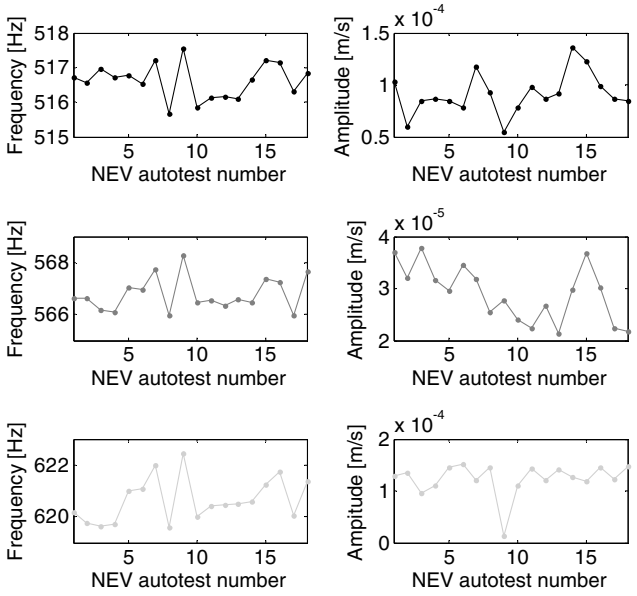

Fig. 6 IMU frequencies (left) and amplitudes (right) as a function of autotest number.

IV. In-Orbit Measured Vibrations

A. Vibration Levels in NEV Orbits

Near-Earth verification (NEV) activity was planned to test PFS health after launch and in conditions not achieved during ground calibration testing. Together with interferogram acquisition, the autotests were recorded as well, allowing the measurement of the speed disturbances just after the spacecraft launch. A total number of 18 autotests were analyzed. Figure 4 shows the speed standard deviation for each of them.

NEV autotests were averaged together to computed the speed spectrum shown in Fig. 5.

Figure 6 provides tracking of the IMU frequencies and amplitudes during NEV activity.

Figure 7 shows rms acceleration levels computed in the frequency range of the reaction wheels and of the gyroscopes. Two curves are provided using the maximum and minimum PFS sensitivities of Table 1.

B. Vibrations During Mars Orbits

The PFS team announced in October 2009 the achievement of one million Mars spectra. Data acquisition started in January 2004 with orbit 10 and is ongoing. Besides the scientific data volume, a large number of autotests was acquired. One autotest per month has been extracted to monitor the evolution of the mechanical vibrations, i.e., starting from orbit number 10 to orbit 11,454, corresponding to the eight years from January 2004 to January 2012. Table 3 reports the orbit number as a function of the year. One orbit is completed in nearly 7.5 h. One must keep in mind that there is a time/data sharing between the payloads; therefore, the PFS is not active on every orbit.

Figure 8 shows the speed standard deviation of the interferometer arms, measured from the PFS autotest for all analyzed orbits.

The tracking of the IMU frequencies and amplitudes over the years is provided in Fig. 9, whereas Table 4 reports the computed Pearson's correlation coefficients between measured amplitudes and frequencies.

Figure 10a provides a detail of the measured speed spectra around 620 Hz for some orbits from numbers 20 to 71. Blowup of the speed spectra from orbit 533 to 680 is shown in Fig. 10b.

Temporal evolution of the reaction wheels and IMU rms accelerations is provided in Fig. 11.

The evidence of the RW disturbances is shown in Fig. 12, where RW harmonics frequencies are superimposed to the spectrograms derived by analyzing the infrared spectra for orbit number 41. The angular momentum M_{ang}, provided by the AOCS of MEX and reported in Fig. 13, were combined with the second-order momentum I_{RW} of each reaction wheel so that the fundamental frequency f_k was computed as a function of time t:

$$f_k(t) = \frac{M_{\text{ang}}(t)}{2\pi I_{\text{RW}}} \tag{2}$$

Moreover, the actual harmonic coefficients were computed by comparison with the measured spectrograms (numbers of each multiple of the fundamental frequency f_k are reported near the curves of Fig. 12).

Finally, the spectrograms of the mechanical vibrations within the 0 to 1300 Hz range and from 450 to 700 Hz are provided in Figs. 14 and 15.

Table 1 Maximum and minimum autotest sensitivities

Frequency, Hz	$S_{\max}$	$S_{\min}$
60	0.6	0.2
110	16.9	6.5
133	31.2	21.5
160	5.2	5.2
390	0.5	0.5
517	21.4	0.9
566	5.2	0.3
617	1.7	0.3
1100	0.3	0.2

Table 2 Acceleration levels measured during microvibration assessment with both IMUs switched on

Disturbance frequency, Hz	*X* axis damper 1, ms^{-2}	*Y* axis damper 1, ms^{-2}	*Z* axis damper 1, ms^{-2}	*X* axis damper 2, ms^{-2}	*Y* axis damper 2, ms^{-2}	*Z* axis damper 2, ms^{-2}
516	0.035	0.026	0.011	0.206	0.095	0.095
570	0.068	0.072	0.133	0.167	0.072	0.121
619	0.029	0.049	0.050	0.027	0.070	0.145

Table 3 Relation between orbit numbers and years

Year	From orbit	To orbit
2004	10	1,200
2005	1,297	2,419
2006	2,531	3,725
2007	3,835	5,026
2008	5,135	6,380
2009	6,420	7,585
2010	7,691	8,736
2011	8,946	10,143
2012	10,304	11,454

C. Discussion

The first analysis considers the evolution of the vibrations for the short time after the launch, i.e., exploiting the measurements taken during the NEV phase. The objective of the analysis was to determine if the first weeks of space environment produced a noticeable effect on the vibration transmission through the spacecraft structure. Considering the speed standard deviation, it remained nearly constant at a level of about 1.6×10^{-4} m/s, as can be seen in Fig. 4.

The speed spectrum of Fig. 5 shows a group of three monoharmonic components spaced about 50 Hz apart in the frequency range from 517 to 622 Hz. These components are due to the IMU's mechanical dithering. The signals at lower frequencies are the RWs' generated disturbances. IMU disturbances are quite stable over time, as shown in Fig. 6, since the vibration amplitudes remained constant versus the "autotest number"; that is to say, versus time. The only exception is the component corresponding to the IMU dithering frequency of 570 Hz that exhibits a sudden vibration amplitude decrease of about 30% during the NEV. The reason for that drop is not clear; a settling in the spacecraft structure can be proposed as culprit, but the fact that the other IMUs' components seem to not be even slightly affected by the change makes this explanation quite unlikely. RMS acceleration levels shown in Fig. 7a are related to the RW vibration in the frequency range from 60 to 400 Hz; it can be shown that the rms is nearly constant, and its average value over time is always within the 0.026 to 0.030 m/s^2 range. Figure 7b shows the vibration levels due to the IMUs. Maximum and minimum rms accelerations vary in the range from 1.4 to 1.7 m/s^2. In both cases,

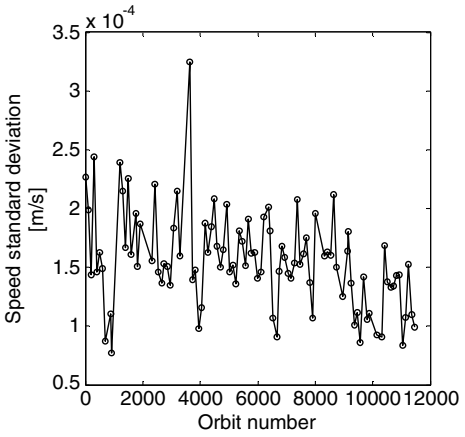

Fig. 8 Standard deviation of the scanning speed for each autotest.

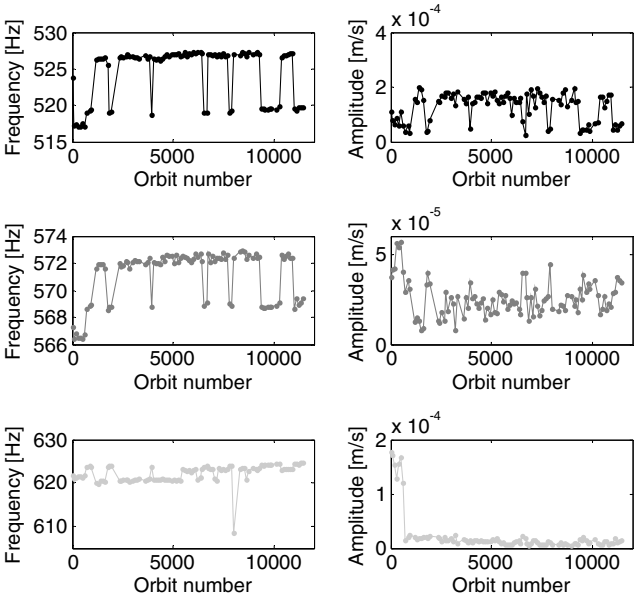

Fig. 9 IMU frequencies and amplitudes change against autotest numbers.

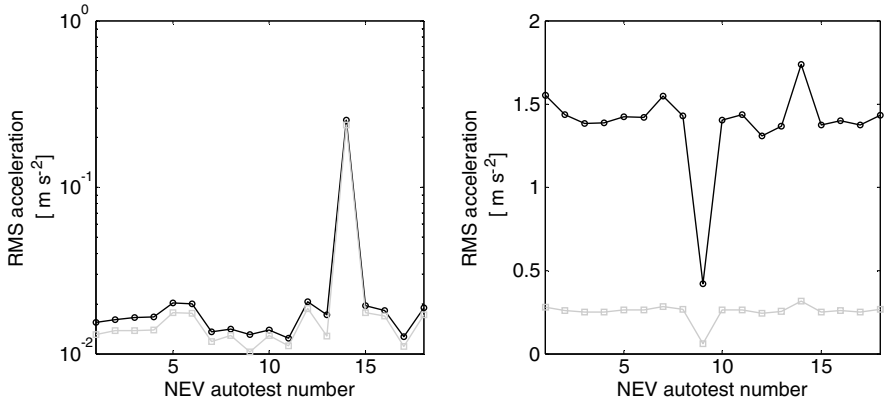

a) RW disturbance within 60–400 Hz range **b) IMU disturbance within 500–650 Hz range**

Fig. 7 RMS equivalent maximum (black) and minimum (gray) acceleration levels during NEV activity.

Table 4 Pearson's correlation coefficients ρ_{xy} for IMU frequencies and amplitudes

Parameter	Value
$x = f_1, y = A_1$	0.87
$x = f_1, y = f_2$	0.95
$x = f_2, y = A_2$	−0.80
$x = f_1, y = f_3$	−0.38
$x = f_3, y = A_3$	−0.12

the rms accelerations can be regarded as constant, with the exception of measurement number 14 that shows a vibration level one order of magnitude larger than the average. Moreover, in a second case (autotest number 9), a reduction by 70% can be highlighted. However, these results are due to changes in the interferometer setting parameters; therefore, the related measurements must be considered as outliers.

The monitoring of the disturbances over the eight years of orbits around Mars is shown in Fig. 8, where it is evidenced that the variability of the overall speed standard deviation in the different orbits remained almost constant over the time, with an average value of 1.6×10^{-4} m/s. Figure 9 provides the tracking of the IMU peak frequencies and peak amplitudes: the main result is a correlation between the first two frequencies and their amplitudes, as shown in Table 4. As mentioned previously, two independent IMUs are present; each IMU is equipped with three gyroscopes having slightly different dithering frequencies around 520, 570, and 620 Hz. During the first orbits (i.e., 20, 37, and 49), both IMUs were switched on, as can be seen by the double peaks in the speed spectrum of Fig. 10a. However, after orbit 49, one of the two IMUs was switched off and the spacecraft operated in nominal mode with only one active and switching between them over the time. This strategy is still used for the MEX spacecraft, but evidently the redundant units are sometimes switched on instead of the nominal ones. This can be seen by looking at Fig. 9, which shows the dithering frequency change in some orbits during the time. The correlation between frequency and amplitude is a consequence of the different FRFs associated with the redundant and nominal IMUs.

The third IMU frequency seems to not be correlated with the other frequencies, as shown in Table 4, and the same conclusion can be drawn for its amplitudes. Actually, computing Pearson's correlation coefficient between the first and third IMU frequencies within the orbits from 1200 to 5346, a high correlation of about 0.85 is achieved. Moreover, the third IMU behaves in a strange manner, because between orbits 633 and 634, as shown in Fig. 10b, its vibration amplitude decreased by 85% and then remained constant for all the time, as seen by the amplitude tracking of Fig. 9. This result is also confirmed by the IMU rms accelerations provided in Fig. 11b, since the maximum and minimum acceleration levels drop around orbit 600. At that point, the rms acceleration limits (maximum and minimum) reduce from 1.6 to 0.56 m/s^2 and from 0.29 to 0.04 m/s^2.

An explanation for this strange behavior has not been identified yet. The most likely explanation is that some change occurred in the spacecraft structure and modified the vibration transmission from IMU to payload, but unfortunately there is no other element supporting this thesis.

The rms acceleration levels in the frequency range of the RW disturbances is almost constant over the years, varying within (0.027 to 0.036) m/s^2. This demonstrates that there is nearly no degradation due to wear of the rolling bearings or other moving parts.

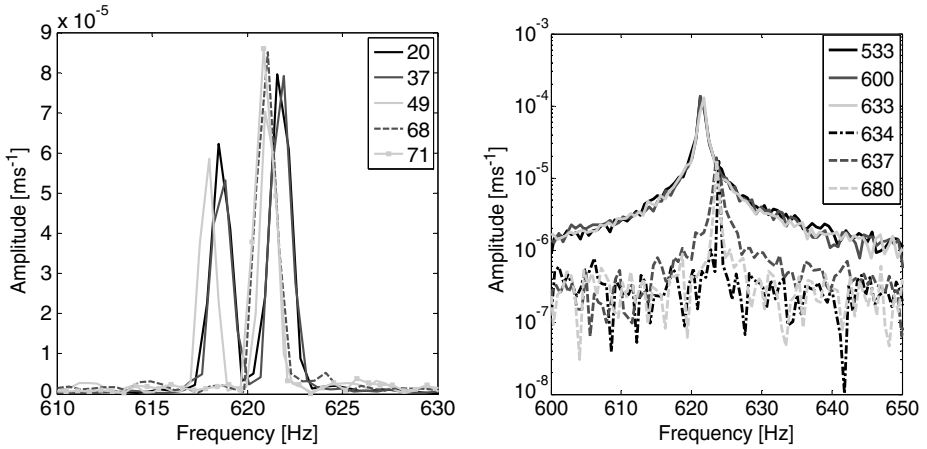

a) Speed spectra from orbits 20 to 71 **b) Speed spectra from orbits 533 to 680**

Fig. 10 Zoom of the measured speed spectra around the third IMU frequency.

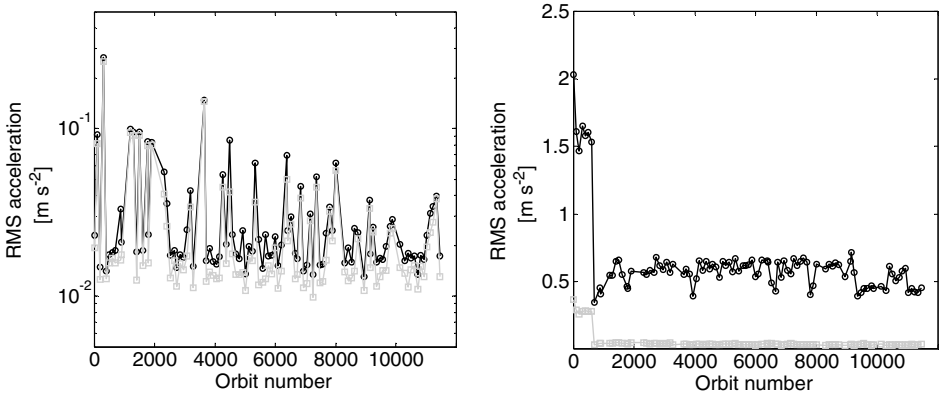

a) RWs disturbance within 60–400 Hz range **b) IMUs disturbance within 500–650 Hz range**

Fig. 11 Tacking over eight years of the rms equivalent maximum (black) and minimum (gay) acceleration levels.

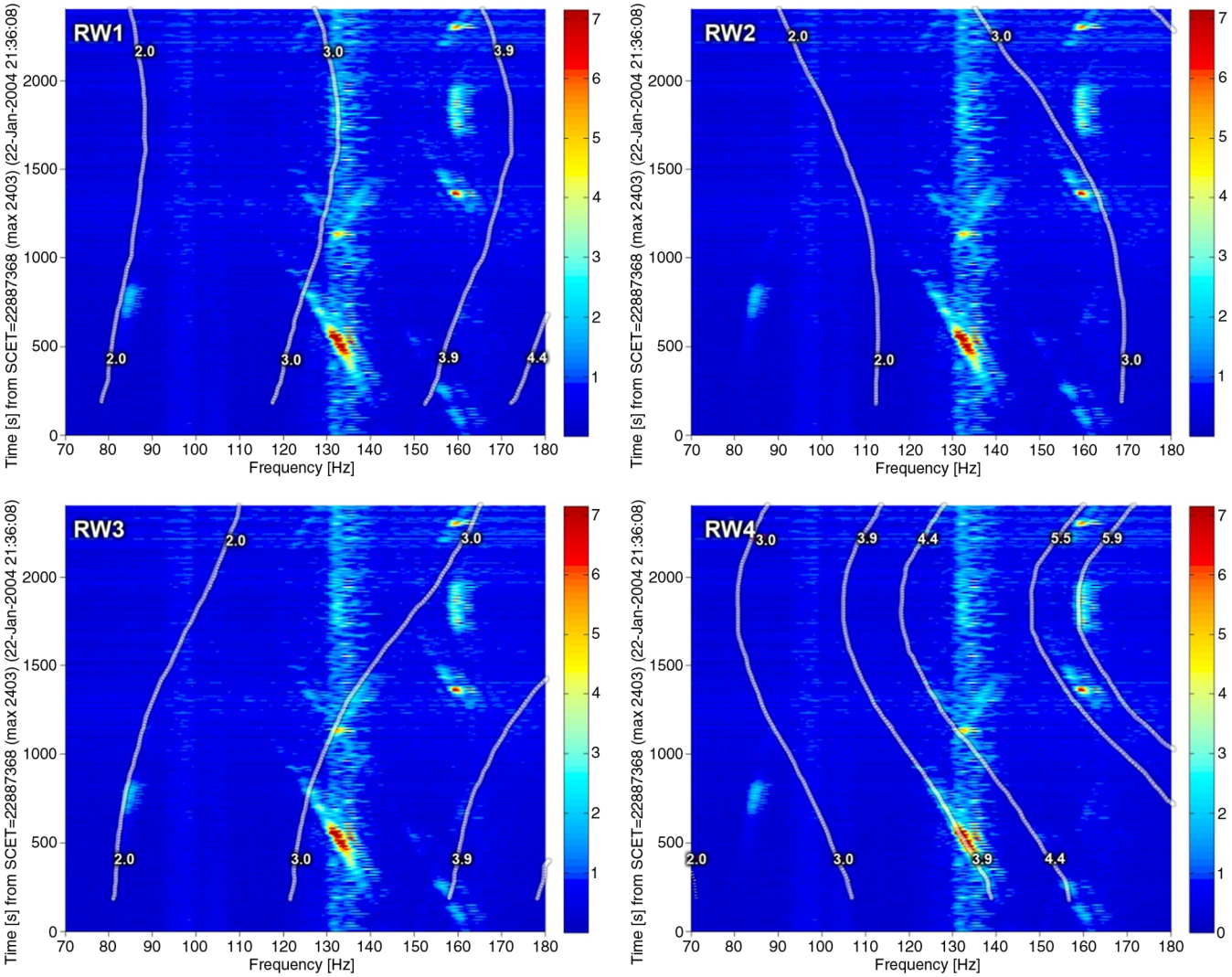

Fig. 12 Spectrograms of mechanical vibrations in range 70–80 Hz during all the observing period of orbit 41 (22 January 2004, duration 40 min) with superimposed data of main harmonics of RWs. Amplitude scale is in relative raw units.

The proof that these spectral lines in the low-frequency range are due to the RW disturbance is provided in Fig. 12, where the spectrograms of mechanical vibrations detected on the measured SW spectra of orbit 41 fit, with high accuracy, the theoretical RW frequencies computed from the angular momentum data provided in Fig. 13. Figure 12 shows clearly that the mechanical vibrations change their frequencies according to those expected from the RW angular momentum data. In PFS spectrograms, higher-order harmonics were also identified, i.e., additional vibration components were found at 2, 3, 3.9, 4.4, 5.5, 5.9, and 7.1 times the fundamental frequency. Moreover, the disturbance amplitudes in the spectrogram change with time because sometimes the forcing frequencies match some structural resonances leading to relevant amplifications. This is evident in Fig. 12: looking to the spectrogram of RW 4, one can see that, when the disturbance frequency (harmonic number 3.9) approaches the PFS resonance (around 133 Hz), the vibration amplitude maximizes.

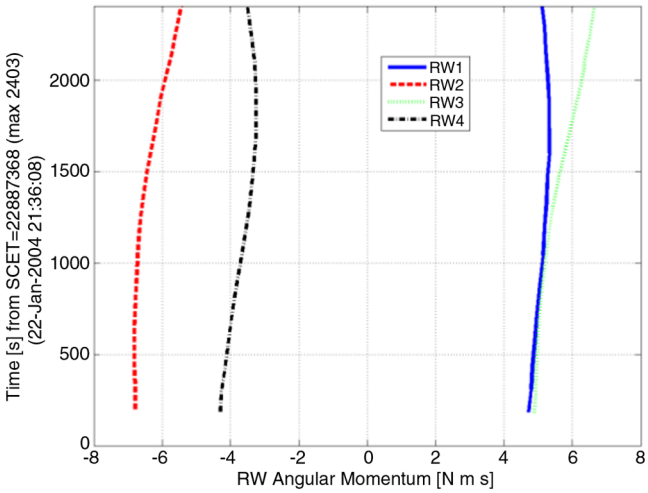

Fig. 13 Angular momentum provided by AOCS of MEX during orbit 41, with the same time scale of Fig. 11.

The spectral analysis of orbit 41 confirms the results derived from the PFS autotest activity. The spectrogram of Fig. 14 highlights that the disturbances spectrum is limited to about 1300 Hz. A similar result is obtained by looking to the average speed spectrum of the NEV activity in Fig. 5. It has to be noted that the faint "shading" of the spectrogram in the range from 1200 to 1300 Hz is actually not deriving from disturbances but is true infrared radiation due to the Mars albedo. Below 1200 Hz, the Mars radiation is negligible and does not "pollute" the vibration information obtained from the SW laser modulation effect. Another disturbance can be noticed around 300 Hz, due to a resonance that derives maybe from the orbiter structure excited by the broadband spectrum vibration of the RWs. The IMU frequency and amplitude during orbit 41 are stable, as

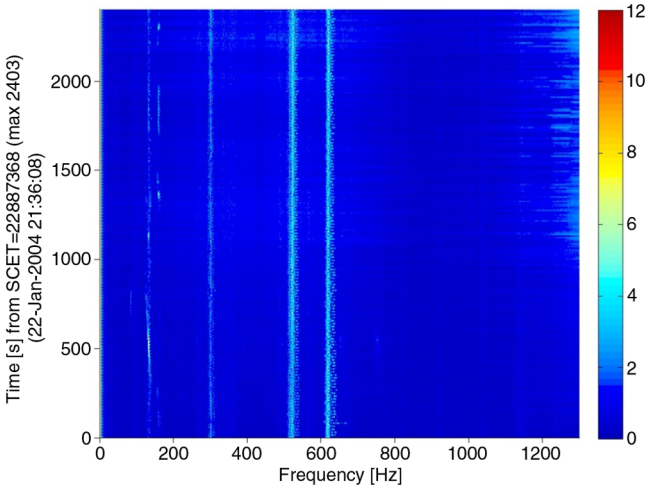

Fig. 14 Spectrogram of mechanical vibrations in range (0 to 1300) Hz, orbit 41. Amplitude scale is in relative raw units.

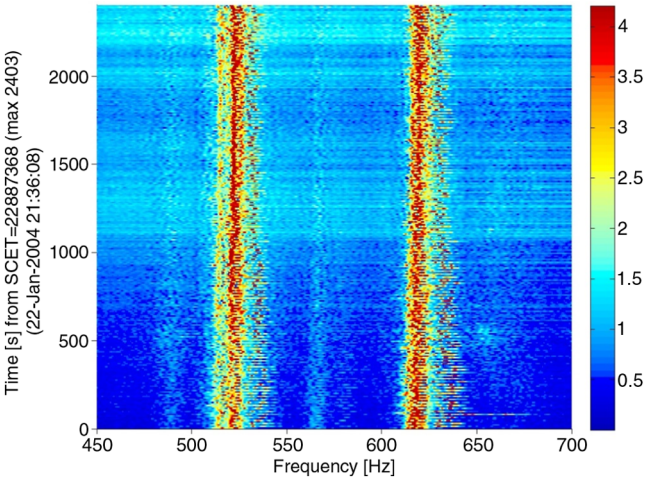

Fig. 15 Spectrogram of mechanical vibrations in range (450 to 700) Hz, orbit 41. Amplitude scale is in relative raw units.

confirmed by Fig. 15 where the three main components are shown. Moreover, it can be seen that the component at about 570 Hz is significantly lower than the other two.

Finally, a complete compatibility was achieved by comparing the measured acceleration levels on the twin spacecraft VEX, during ground testing (with rms acceleration varying within (0.19 to 0.37) m/s^2 range); and the MEX, with the inflight data of Figs. 7b and 11b.

V. Conclusions

This work monitors the vibration environment onboard the Mars Express spacecraft from its checkout phase immediately after launch to its long active phase in orbit around Mars. The acceleration levels have been measured, exploiting the planetary Fourier spectrometer sensitivity to the mechanical disturbances. The main vibration sources were found to be the spacecraft inertial measurement units and the reaction wheels, with different excitation bandwidths respectively at (510 to 630) Hz and (20 to 400) Hz. The disturbances from the inertial measurement units have stable frequencies and amplitudes, whereas the reaction wheels show variable frequency content and amplitudes depending on their rotational speed deriving from the spacecraft's maneuvers. Moreover, the tracking of the vibrations' characteristics over time shows that both the disturbances deriving from the inertial measurement units and the reaction wheels are almost constant; therefore, no evident change of the spacecraft characteristics is evident. Finally, derived acceleration levels in flight were demonstrated to be fully compatible with those obtained from the ground testing activity.

The data provided as a result of this activity, both in terms of amplitude and frequency, can be used as an initial guess for the design of vibration sensitive payloads, although with the limit of being mainly representative of the Mars Express and Venus Express spacecraft.

Acknowledgments

The authors thankfully acknowledge the financial support provided by the Italian Space Agency (ASI) in the framework of the research program "PFS for Mars Express" and Vittorio Formisano, the planetary Fourier spectrometer Principal Investigator at the time of instrument development and launch.

References

[1] Dyne, S., Tunbridge, D., and Collins, P., "The Vibration Environment on a Satellite in Orbit," *IEE Colloquium on High Accuracy Platform Control in Space*, IET, 1993, pp. 12/1–12/6.

[2] Le Duigou, J.-M., "SM98-030/431 Microvibration Measurements on Spot 4, Results of the Micromedy Experiment," *Spacecraft Structures, Materials and Mechanical Testing*, Vol. 428, 1999, p. 475.

[3] Ooi, Y., Kamiya, T., Jono, T., Takayama, Y., and Yamawaki, T., "Evaluation of Ground and Orbit Microvibration of OICETS," *17th IFAC Symposium on Automatic Control in Aerospace*, Vol. 17, IFAC Secretariat, Toulouse, France, 2007, pp. 265–270.

[4] Laurens, P., Decoux, E., and Janvier, M., "SOHO Microvibrations: Analyses, Tests and Flight Results," *Spacecraft Guidance, Navigation and Control Systems*, Vol. 381, 1997, p. 489.

[5] Giuranna, M., Formisano, V., Biondi, D., Ekonomov, A., Fonti, S., Grassi, D., Hirsch, H., Khatuntsev, I., Ignatiev, N., Michalska, M., Mattana, A., Maturilli, A., Moshkin, B. E., Mencarelli, E., Nespoli, F., Orfei, R., Orleanski, P., Piccioni, G., Rataj, M., Saggin, B., and Zasova, L., "Calibration of the Planetary Fourier Spectrometer Short Wavelength Channel," *Planetary and Space Science*, Vol. 53, No. 10, 2005, pp. 975–991. doi:10.1016/j.pss.2004.12.007

[6] Giuranna, M., Formisano, V., Biondi, D., Ekonomov, A., Fonti, S., Grassi, D., Hirsch, H., Khatuntsev, I., Ignatiev, N., Malgoska, M., Mattana, A., Maturilli, A., Mencarelli, E., Nespoli, F., Orfei, R., Orleanski, P., Piccioni, G., Rataj, M., Saggin, B., and Zasova, L., "Calibration of the Planetary Fourier Spectrometer Long Wavelength Channel," *Planetary and Space Science*, Vol. 53, No. 10, 2005, pp. 993–1007. doi:10.1016/j.pss.2005.02.007

[7] Davis, S. P., Abrams, M. C., and Brault, J. W., *Fourier Transform Spectrometry*, Elsevier, New York, 2001.

[8] Comolli, L., and Saggin, B., "Mechanical Vibrations Onboard Mars Express Orbiter Detected by the Fourier Spectrometer "PFS"," *XX AIDAA Congress*, Milan, 2009.

[9] Comolli, L., and Saggin, B., "Analysis of Disturbances in the Planetary Fourier Spectrometer Through Numerical Modeling," *Planetary and Space Science*, Vol. 58, No. 5, 2010, pp. 864–874. doi:10.1016/j.pss.2010.01.011

[10] Wacker, T., Weimer, L., and Eckert, K., "GOCE Platform Micro-Vibration Verification by Test and Analysis," *European Conference on Spacecraft Structures, Materials and Mechanical Testing*, ESA, Noordwijk, The Netherlands, 2005, pp. 733–740.

[11] Drisch, H. P., "Thermally Induced Vibrations of Long Thin-Walled Cylindes of Open Section," *Journal of Spacecraft and Rockets*, Vol. 7, No. 8, 1970, pp. 897–905. doi:10.2514/3.30068

[12] Pavarin, D., Francesconi, A., Destefanis, R., Lambert, M., Bettella, A., Debei, S., Cecco, M. D., Faraud, M., Giacomuzzo, C., Marucchi-Chierro, P. C., Parzianello, G., Saggin, B., and Angrilli, F., "Acceleration Fields Induced by Hypervelocity Impacts on Spacecraft Structures," *International Journal of Impact Engineering*, Vol. 33, Nos. 1–12, 2006, pp. 580–591. doi:10.1016/j.ijimpeng.2006.09.060

[13] Lawrence, A., *Modern Inertial Technology: Navigation, Guidance, and Control*, 2nd ed., Springer–Verlag, New York, 1998.

[14] Siouris, G. M., "Aerospace Avionics Systems: A Modern Synthesis," Academic Press, New York, 1993.

[15] Liebold, F., Wiegand, S., and Kaso, R., "Reaction Wheel Disturbance Characterization by Analysis of Micro-Vibration Measurements," *3rd*

International Conference on Mechanical and Aerospace Engineering (ICMAE), Vol. 232, Trans Tech Publ., Paris, 2012, pp. 445–449.

[16] Kamesh, D., Pandiyan, R., and Ghosal, A., "Passive Vibration Isolation of Reaction Wheel Disturbances Using a Low Frequency Flexible Space Platform," *Journal of Sound and Vibration*, Vol. 331, No. 6, 2012, pp. 1310–1330. doi:10.1016/j.jsv.2011.10.033

[17] Liu, K.-C., Maghami, P., and Blaurock, C., "Reaction Wheel Disturbance Modeling, Jitter Analysis, and Validation Tests for Solar Dynamics Observatory," *AIAA Guidance, Navigation and Control Conference and Exhibit*, AIAA Paper 2008-7232, 2008.

[18] Bronowicki, A. J., "Vibration Isolator for Large Space Telescopes," *Journal of Spacecraft and Rockets*, Vol. 43, No. 1, 2006, pp. 45–53. doi:10.2514/1.12036

[19] Toyoshima, M., Jono, T., Takahashi, N., Yamawaki, T., Nakagawa, K., and Arai, K., "Transfer Functions of Microvibrational Disturbances on a Satellite," *21st International Communications Satellite Systems Conference and Exhibit*, AIAA Paper 2003-2406, 2003.

[20] Masterson, R. A., Miller, D. W., and Grogan, R. L., "Development and Validation of Reaction Wheel Disturbance Models: Empirical Model," *Journal of Sound and Vibration*, Vol. 249, No. 3, 2002, pp. 575–598. doi:10.1006/jsvi.2001.3868

[21] De Weck, O., "Reaction Wheel Disturbance Analysis," Massachusetts Inst. of Technology, Memo. MIT-SSL-NGST-98-1, Cambridge, MA, 1998.

[22] Saggin, B., Comolli, L., and Formisano, V., "Mechanical Disturbances in Fourier Spectrometers," *Applied Optics*, Vol. 46, No. 22, 2007, pp. 5248–5256. doi:10.1364/AO.46.005248

[23] Svedhem, H., Titov, D. V., Mc Coy, D., Lebreton, J. P., Barabash, S., Bertaux, J. L., Drossart, P., Formisano, V., Hausler, B., Korablev, O., Markiewicz, W. J., Nevejans, D., Patzold, M., Piccioni, G., Zhang, T. L., Taylor, F. W., Lellouch, E., Koschny, D., Witasse, O., Eggel, H., Warhaut, M., Accomazzo, A., Rodriguez-Canabal, J., Fabrega, J., Schirmann, T., Clochet, A., and Coradini, M., "Venus Express: The First European Mission to Venus," *Planetary and Space Science*, Vol. 55, No. 12, 2007, pp. 1636–1652. doi:10.1016/j.pss.2007.01.013

J. Domber
Associate Editor